Targetry and Collection Problems

A. Van Ginneken
Fermi National Accelerator Laboratory*
P. O. Box 500, Batavia, IL 60510

June 1999

1 Introduction

This note brings attention to some problems encountered in comparing recent results from decay channel tracking (using the code of ref. [1]) vis-a-vis the Status Report [2]. In particular the 'low-energy, long-bunch' example of the Status Report is examined in some detail. Plausible explanations for the discrepancies encountered are commented upon below. While these discrepancies suggest significant lower yields they are not so severe as to seriously impair this phase of the project. Even if the lesser yields prove to be unacceptable there are alternatives, such as those achieved by means of higher gradients in the decay pipe.

In addition, this note provides a comparison between muon capture yields for 1 *nsec vs* 3 *nsec* wide beams for the same decay channel as well as a comparison between capture yields for the 'narrow' $r = 15\ cm/B = 5\ T$ channel *vs* the 'wide' 30/1.25 decay pipe. For these last two topics the study here is again confined to the low-energy example from the Status Report and results are presented here mostly for intercomparison and by way of illustration. It is clear that one would need to re-optimize the entire decay channel (placement of cavities, gradients, frequencies, etc.) if one were to adopt a 3 *nsec* proton driver beam and/or a wider decay pipe. All of this is very much unfinished business but reviews scheduled for the near future prompt summarizing some of this now.

*Work supported by the U.S. Department of Energy under contract No. DE-AC02-76CHO3000.

2 Comparison with Status Report

The main aim here is to study the 'low-energy, long-bunch' example of the phase rotation as presented in [2]. Placement, gradient, and frequency of each cavity gap (represented in the program as simple kicks) is from table IV and fig. 20 of [2] and is reproduced in table 1 here. The first column gives the distance, z, in cm, of each cavity along the 40 m long decay pipe with, next, its frequency (ν in MHz) followed by the $maximum$ energy 'kick' (in MeV) it can deliver in the simulation. The main decay pipe solenoid is assumed to have a 15 cm radius with a 5 T field (this is not explicit in the Status Report but appears in ref. [3] which corresponds to ref. [52] quoted in [2]).

The main difference between the present simulations and those of [2] is in particle production. Ref. [2] assumes a copper target (unspecified length, 1 cm radius) tilted at 150 $mrad$ with respect to the solenoid axis and uses the ARC [4] code to predict pion production. The present exercise uses a 36 cm long, 1 cm radius gallium target and relies on MARS [5] for pion generation. The target is placed in a 20 T solenoid field and—in this study—is either along the solenoid axis or tilted at 200 $mrad$ to the axis [6]. Between target and main solenoid is a transition solenoid which reduces the field adiabatically [7] over a distance of 204 cm. Ref. [2] reports 0.39 muons per incident proton in a phase space region $0.06 \leq E_{kin} \leq 0.20$ GeV/c by $3 \leq ct - z \leq 11$ m, where t is arrival time at distance, z, in this case at the end of the channel. In the present study the muon yield within a box of the same size is maximized by varying the timing of the individual RF cavities and by moving the 'collection box' about in E–t–space. This maximization is performed for the case where the target is tilted at 200 mrad to the axis and where π^+/μ^+ are collected. The other cases are run with the same RF phases. Yields for these should therefore improve somewhat if they were separately optimized. Timings shown in columns four and five of table 1 specify where the RF sine wave vanishes (times are multiplied by c and expressed in cm) for the two cases with differing solenoid radius and field (in cm and $Tesla$) which are displayed in the header. For collection of negative particles the phase is displaced by π radians.

Table 2 collects some information gathered from a set of Monte Carlo runs for the 15 cm/5 T channel. The first three columns indicate the parameters of the run: whether μ^+ or μ^- are collected, time spread of the 16 GeV proton beam in nanoseconds, and tilt angle—if any—of the target with respect to the channel axis in milliradians. The next two columns refer to total yields of muons and (undecayed) pions of the indicated sign. The

Table 1: Position along Decay Line (z in cm), Frequency (ν in MHz), Maximum Energy Increase (ΔE in MeV), and Timing (ct in cm) of RF Cavities for $r = 15cm/B = 5T$ and $r = 30cm/B = 1.25T$ solenoids.

z	ν	ΔE	15/5	30/1.25	z	ν	ΔE	15/5	30/1.25
300	60	6.0	325.0	325.0	2220	30	4.8	2504.6	2493.0
340	60	6.0	372.1	371.1	2340	30	4.8	2637.4	2625.6
380	60	6.0	418.9	418.2	2460	30	4.8	2769.9	2758.2
420	30	4.8	465.4	464.4	2580	30	4.8	2902.0	2890.3
540	30	4.8	604.3	602.3	2700	30	4.8	3033.9	3022.2
660	30	4.8	742.8	739.7	2820	30	4.8	3165.5	3153.9
780	30	4.8	880.8	876.7	2940	30	4.8	3296.9	3285.3
900	30	4.8	1018.4	1013.4	3060	30	4.8	3428.0	3416.6
1020	30	4.8	1155.6	1149.6	3180	30	4.8	3558.8	3547.6
1140	30	4.8	1292.3	1285.5	3300	60	4.8	3689.5	3678.5
1260	30	4.8	1428.6	1420.9	3420	60	4.8	3819.9	3809.0
1380	30	4.8	1564.5	1556.1	3540	60	4.8	3950.1	3939.4
1500	30	4.8	1700.0	1690.9	3660	60	4.8	4080.1	4069.6
1620	30	4.8	1835.1	1825.3	3780	37	4.8	4210.7	4119.5
1740	30	4.8	1969.7	1959.5	3900	37	4.8	4339.7	4329.3
1860	30	4.8	2104.0	2093.3	4020	37	4.8	4469.2	4458.9
1980	30	4.8	2237.9	2226.8	4140	37	4.8	4598.4	4588.3
2100	30	4.8	2371.4	2360.0					

Table 2: Yields, Restricted Emittances, Average Momentum and *rms* Spread at End of r=15 cm, B=5 T Channel. Units are *cm* and *radian* to appropriate powers and GeV/c.

case			*total*		*within cut*					
	ns	mrad	μ	π	μ	ϵ_6^N	ϵ_T^N	ϵ_L^N	$< p >$	σ_p
+	1	0	0.386	0.142	0.218	161	1.53	67.0	0.275	0.035
—	1	0	0.354	0.115	0.214	155	1.54	65.7	0.275	0.034
+	1	200	0.391	0.105	0.243	174	1.55	66.3	0.275	0.034
—	1	200	0.373	0.097	0.236	180	1.68	64.4	0.278	0.034
+	3	0	0.386	0.143	0.196	164	1.54	69.2	0.277	0.037
—	3	0	0.353	0.116	0.195	163	1.54	68.6	0.278	0.037
+	3	200	0.390	0.104	0.219	187	1.64	69.6	0.279	0.037
—	3	200	0.375	0.095	0.214	195	1.70	67.5	0.279	0.036

average energy of the latter is rather high and therefore one does not expect them to make a substantial contribution to muon yield within the cuts—were one to extend the channel. The remaining columns pertain to muons within the $0.13 \leq E_{kin} \leq 0.27\ GeV$ by $2 \leq ct - z \leq 10\ m$ box: yield, 6-D emittance, average transverse emittance, longitudinal emittance, average momentum, and *rms* spread of the latter. All emittances are normalized and units are centimeter and radian to their appropriate powers. The 6-D-emittance, ϵ_6^N, is obtained as the square root of the 6-D-determinant of the correlation matrix of the phase space variables. Average transverse emittance, $\langle \epsilon_T^2 \rangle^{1/2}$, abbreviated as ϵ_T^N in the table, is calculated as the 4th root of the 4-D-determinant of the transverse phase space variables—a procedure which removes angular momentum correlations. (If no correlations are present ϵ_T^N is the geometric mean of the normalized x and y transverse emittances.) Longitudinal emittance, ϵ_L^N, is the square root of the determinant of the E–t matrix. The last two columns are average muon momentum and standard deviation of the distribution about the average, in GeV.

Fig. 1 shows the progression of the $\pi\mu$ cloud through the channel (for the case where μ^+ are collected, 1 *nsec* wide proton beam, and tilted target) in the form of E–t phase space plots at various points along the way. In each frame a curve is superimposed which shows the RF energy gain experienced by a particle in the cavity encountered just prior to where the phase space is recorded. It is shown centered on the central energy of the cut (left

scale) and calibrated in MeV (right scale). The last frame represents the situation at the end of the channel and is reproduced in fig. 2 with the box-like superimposed and with projections of the 2-D-distribution on the coordinate axes. Fig. 3 is similar to fig. 1, but is confined to the π and μ which pass the final cut. The first frame of fig. 3 shows how one is quite sensitive to pions produced at low energy.

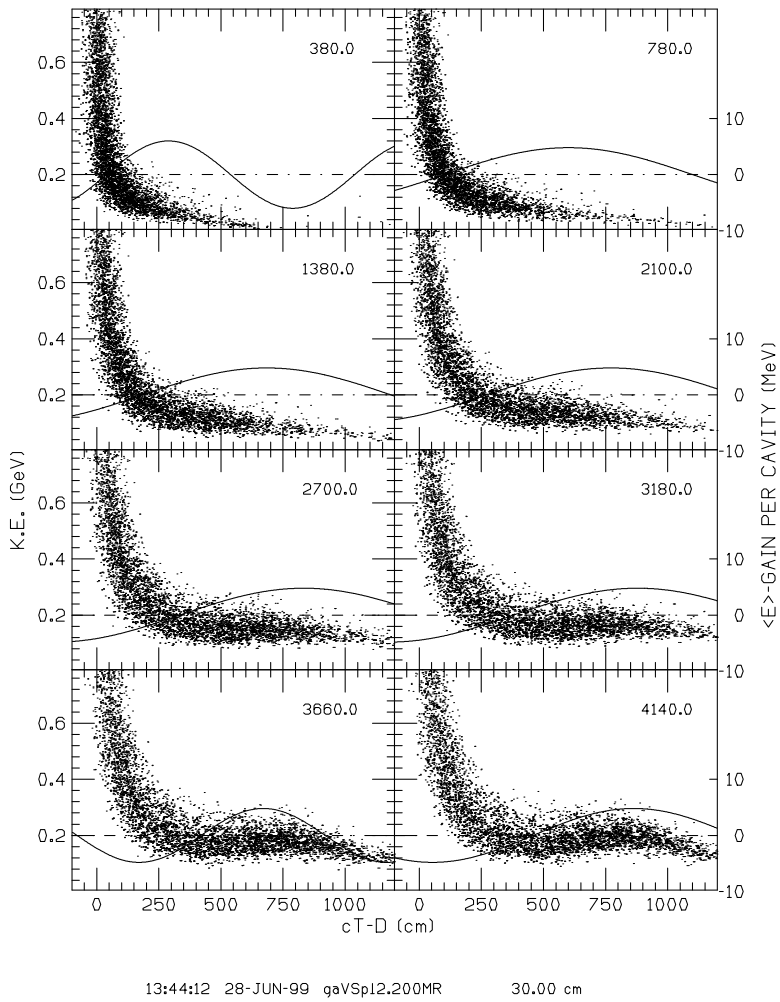

Figure 1: E–t phase space of all pions and muons which remain inside pipe at various points along the channel. The curve represents the energy gain of the particles in the cavity traversed just before being recorded (right scale).

From table 2 it can be seen that the maximum yield (within the cuts)

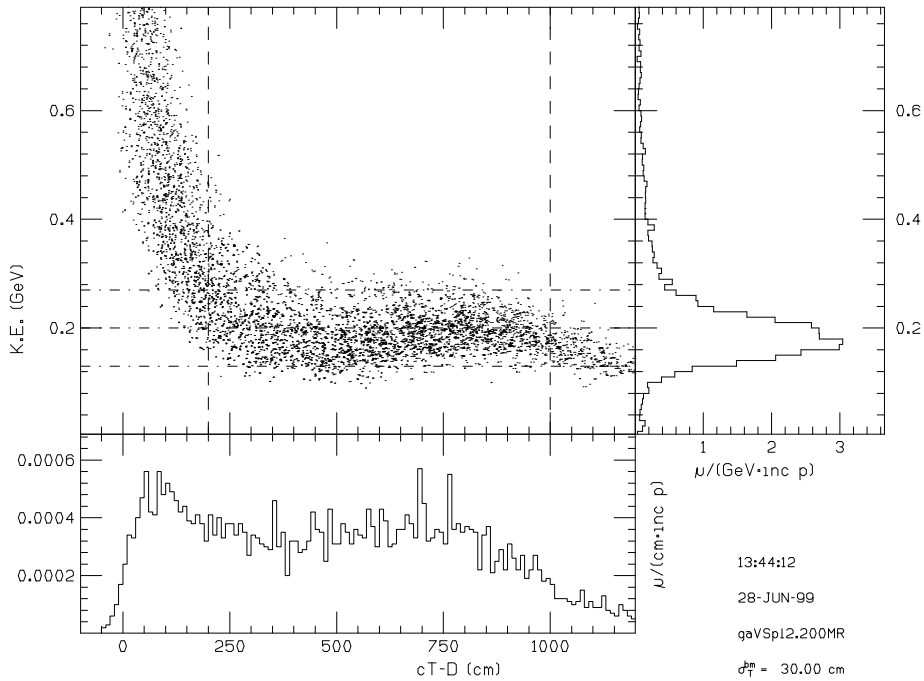

Figure 2: Last frame of fig. 1 with acceptance cuts superimposed and with E and t projections.

is 0.24 μ^+ compared to 0.39 reported in [2]. The location of the box is also quite different from [2]: in the present study one is compelled to collect at a higher energy. Comparing fig. 18 of [2] with fig. 2 above suggests the former has a much smaller emittance of the beam within its box. Indeed the standard deviations on t and E reported in [2] give an approximate longitudinal emittance of 3.5 $GeV \cdot cm$ versus 6.9 $GeV \cdot cm$ for $\sigma_E \cdot \sigma_t$ in the present case. A smaller collection box (0.07 $GeV \times 6$ m and concentric with the 0.14×8 one, above) contains 0.305 μ's with $\epsilon_L \approx 2.0$ $GeV \cdot cm$ according to [2]. A similar exercise done here yields only 0.138 μ's and with $\epsilon_L \approx 3.0$ $GeV \cdot cm$ in a box centered at (0.185 GeV, $7m$) which is located well off-center from the larger box at (0.2 GeV, 6 m). It is clear from fig. 2 that a concentric box would collect considerably less.

These discrepancies may be related to differences in target material, tilt angle, and incident proton energy (24 or 30 GeV *vs* 16). Of these, the last is quite significant: if 30 GeV is in fact used in [2] it may account for a factor of about 1.5 in yield (see, e.g., fig. 16 in [2]) and—by this rather crude measure—the discrepancy then amounts to no more than 10%. Another

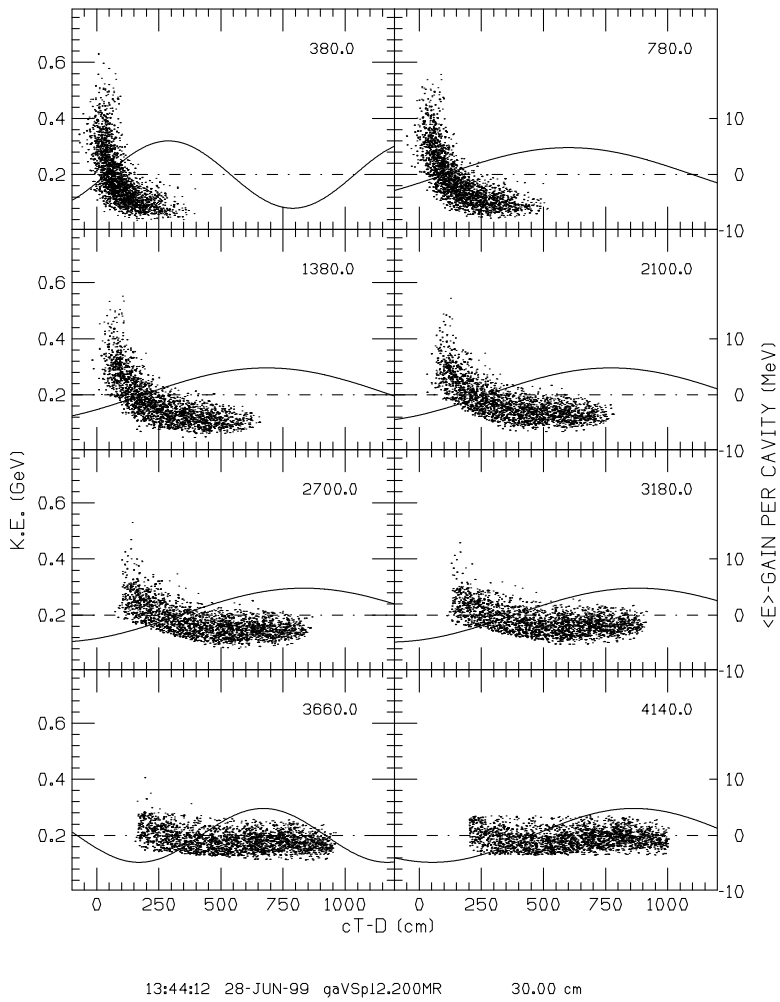

Figure 3: Same as fig. 1 but restricted to those pions and muons which satisfy the cuts at the end of the channel.

source of disparity is the use of MARS here *vs* ARC in [2]. Comparison of ARC and MARS predictions [8] shows that ARC results exhibit strong peaking in the pion spectra below about 0.15 GeV where it exceeds MARS predictions by as much as a factor of two (π^+) or three (π^-). Above 0.15 GeV pion energy the roles are reversed and MARS spectra lie above those of ARC. This suggests that the higher yield, lower average energy, and smaller longitudinal emittance inside the cuts correlate strongly with the low energy peak exhibited in the ARC pion spectra. Which program has the best predictive

Table 3: Yields, Restricted Emittances, Average Momentum and *rms* Spread at End of r=30 cm, B=1.25 T Channel. Units are *cm* and *radian* to appropriate powers and GeV/c.

case			*total*		*within cut*					
	ns	mrad	μ	π	μ	ϵ_6^N	ϵ_T^N	ϵ_L^N	$< p >$	σ_p
+	1	0	0.289	0.073	0.193	179	1.83	53.3	0.253	0.029
—	1	0	0.274	0.060	0.188	177	1.83	52.7	0.254	0.029
+	1	200	0.299	0.055	0.215	203	1.96	52.7	0.254	0.029
—	1	200	0.286	0.051	0.212	207	2.00	51.7	0.255	0.029
+	3	0	0.289	0.073	0.177	210	1.85	61.3	0.255	0.034
—	3	0	0.273	0.062	0.172	207	1.85	60.4	0.256	0.034
+	3	200	0.298	0.054	0.198	235	1.98	60.2	0.258	0.034
—	3	200	0.286	0.051	0.195	231	1.98	58.9	0.257	0.033

power in this instance is to be decided experimentally but detailed results for these low pion energies are not readily available. Note however that MARS agrees well with experiment at higher pion momenta, is much closer than ARC to predictions of the DPMJET program [9], and is more empirically motivated than ARC. For now, the conclusion is that one must attach considerable uncertainty to the 0.39 and 0.305 μ/proton and to the phase space picture presented in fig. 18 of [2] for the low-energy, long bunch example.

3 Lower Field Decay Channel

Present thinking favors a larger radius (30 cm), lower field (1.25 T) decay channel over the 15 $cm/5\ T$ example referred to above. Therefore the above exercises are repeated for the wider channel case. As in the 15 $cm/5\ T$ example, RF phasing and location of the cuts is allowed to vary so as to optimize muon yield within the box. Otherwise, positions, frequencies, and gradients of the RF are identical to those of [2]. The timing adopted is also given in table 1 (cols. 5 and 10). Table 3 shows yield deteriorates by about 10% compared with the high-field results of table 2.

Fig. 4 shows the final E–t-phase space for μ^+ from a 1 nsec proton beam on a 200 mrad tilted target in the wide channel. One source for the decline in yield is related to the p_T-kick given the muon from π-decay. The kick

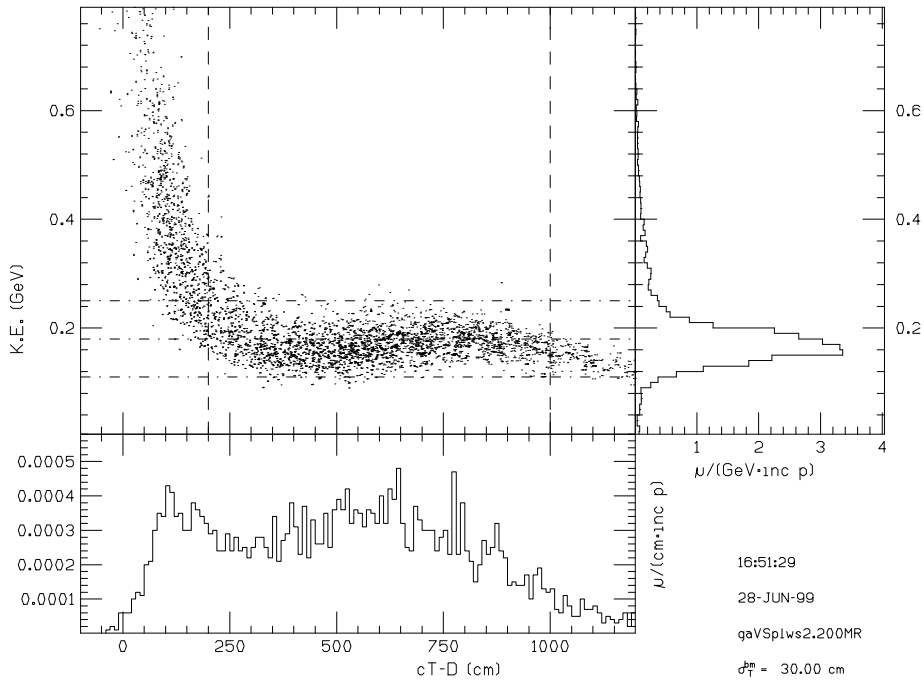

Figure 4: E–t phase space at the end of r=30 cm, 1.25 T decay channel. Other parameters are same as in fig. 1.

may be as large as $p_{dec} = 0.03\ GeV/c$ which, for a particle traveling parallel to the solenoid axis, would result in a Larmor radius four times larger in the weaker field: 8 cm *vs* 2 cm. When $p_T^\pi \neq 0$ the worst case occurs when p_{dec} adds algebraically to p_T^π and when the decay kick shifts the guide center of the Larmor motion shifts radially outward. Ignoring the guide center shift—which should roughly balance out—and assuming the decay pipe is uniformly filled with pions, results in a loss of 25% of all muons in the 5 T channel *vs* 46% in the 1.25 T 'worst case'. The actual situation is not nearly as bad because the p_T add vectorially and the pions are denser in the center of the pipe due to scraping and because they are produced there. A more appropriate measure might be to compare transverse emittance growth of the muon 'beam' due to the decay kick, $\Delta\epsilon_T^N \approx \beta_T \frac{\langle\theta^2\rangle}{2}\beta\gamma$, with the average transverse emittance of the muons collected (ϵ_T^N in tables 2 and 3). In the formula for $\Delta\epsilon_T^N$, β_T is the betatron function while β and γ are the usual relativistic variables. The mean square angle incurred at decay $\langle\theta^2\rangle = p_{dec}^2/3p_\mu^2 \approx 0.004$ for the p_μ encountered here. This results in $\Delta\epsilon_T^N/\epsilon_T^N$ of about 8% for the 5 T channel versus about 24% for the 1.25 T solenoid using

values of β_T, p_μ and ϵ_T^N from the Monte Carlo.

Other factors contribute to the decline in yield: a weaker field in the main solenoid means that a transition solenoid of the same dimensions connecting to the same 20 T solenoid provides a poorer match. Again, since frequency, gradient, etc., are optimized to the 5 T channel, yields for the 1.25 T channel would necessarily improve with a separate optimization.

4 Proton Driver Pulse Length

The pulse length of the proton driver may be expected to influence the collection efficiency in the decay channel. How strong an influence will depend mainly on the RF-frequencies employed in the channel—especially near the beginning. In Tables 2 and 3 results for muon collection for a $\sigma_t = 3$ *nsec* beam are exhibited along with those for a 1 *nsec* beam. For the 15 $cm/5\ T$ case, fig. 5 displays—similarly to fig. 2—the situation at the end of the channel when the proton beam is widened to 3 *nsecs*. Collection efficiencies are seen to be down about 10% across the board. This penalty

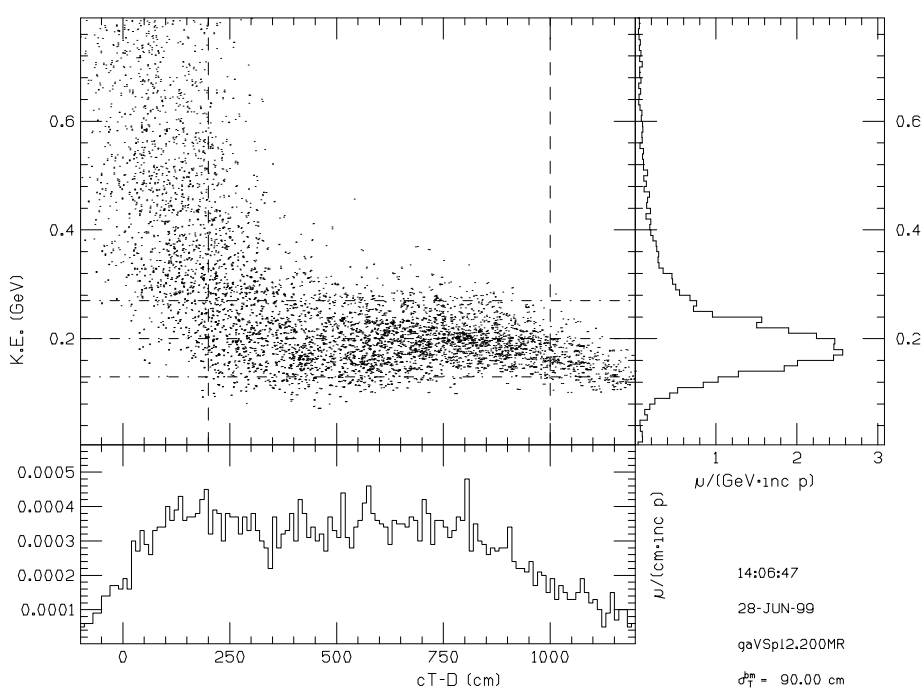

Figure 5: E–t phase space at the end of r=15 cm, B=5 T decay channel for 3 *nsec* long proton driver pulse (*vs* 1 *nsec* in fig. 2).

could again be reduced if channel parameters were optimized for 3 *nsec* rather than 1 *nsec* bunches.

5 Concluding Remarks

Serious discrepancies are encountered in trying to reproduce the results of the 'low-energy long-bunch' example of the Status Report. It must be emphasized that the main concern is not just about numbers of muons collected but about the phase space they occupy within the cuts. It is likely that the low-energy scenario of the Status Report either needs to be amended or else be backed up by more investigation into the validity of ARC as applied in this situation. Using a channel with lower field, larger radius reduces yields by about 10%. Likewise, using longer (3 *nsec*) proton driver bunches in this scenario lowers yields by about 10% from the 1 *nsec* case.

My thanks to N. Holtkamp and D. Neuffer for their helpful comments.

References

[1] A. Van Ginneken and D.V. Neuffer, Nucl. Inst. Meth. **A425**, 165 (1999).

[2] C. Ankenbrandt et al., Fermilab-Pub-98/179, submitted to Physical Review (1998).

[3] R. Palmer et al., *Muon Collider Design*, BNL-62949 (1996).

[4] S. H. Kahana, Y. Pang and T.J. Schlagel, in *Proc. Heavy Ion Physics at the AGS-HIPAGS '93*, G. S. F. Stephans et al. Eds., (1993); D. Kahana and Y. Torun, *Analysis of Pion Production Data from E-802 at 14.6 GeV/c Using ARC*, BNL-61983 (1995).

[5] N. V. Mokhov, *The* MARS *Code System User's Guide, version 13 (95)*, FNAL-FN-628 (1995).

[6] These were chosen from among available files, which are courtesy of N. V. Mokhov.

[7] N. V. Mokhov, R. J. Noble, and A. Van Ginneken, *Target and Collection Optimization for Muon Colliders*, AIP Conf. Proc. *372*, 61 (1996).

[8] N. V. Mokhov ans S. I. Striganov, FNAL-Conf-98/053 (1998).

[9] J. Ranft, Phys. Rev., **D51**, 64 (1995); —, Gran Sasso Rept. INFN/AE-97/45 (1997).